Review Article

Saleh M. Bufarwa*, Reem M. El-Sefait, Dalal K. Thbayh, Mustapha Belaidi, Rehab K. Al-Shemary, Rema. M. Abdusamea, Marei M. El-Ajaily, Béla Fiser, Hanan A. Bader, Abdulsalam A. Saleh and Mohamad M. Bufarwa

Antituberculosis, antimicrobial, antioxidant, cytotoxicity and anti-inflammatory activity of Schiff base derived from 2,3-diaminophenazine moiety and its metal(II) complexes: structural elucidation, computational aspects, and biological evaluation

https://doi.org/10.1515/revic-2024-0007 Received January 24, 2024; accepted July 1, 2024; published online July 29, 2024

Abstract: Enticed by the present scenario of infectious diseases, four new Co(II), Ni(II), Cu(II), and Cd(II) complexes of Schiff base ligand were synthesized from 6,6'-((1E-1' E)(phenazine-2,3-dielbis(azanylidene)-bis-(methanylidene)-bis-(3-(diethylamino)phenol)) ($\mathbf{H_2L}$) to ascertain as effective drug for antituberculosis, anti-inflammatory, antioxidant, cytotoxic and antimicrobial activities. The organic ligand and its metal(II) complexes were characterized by numerous

physical and spectroscopic methods, which showed that the complexes have a general formula, [ML], (where M = Co(II) (C1), Ni(II) (C2), Cu(II) (C3) and Cd(II) (C4)), for metal complexes have been proposed and have a square planar geometry, are amorphous in nature, and are thermally stable. Data highlight obtained from activity testing against tuberculosis, inflammation, and oxidants that all compounds are significantly active against these symptoms. Also, was to evaluate the effectiveness of various compounds against bacterial and fungal strains. Specifically, four bacterial strains (*Bacillus subtilis, Staphylococcus aureus, Escherichia coli*, and *Pseudomonas aeruginosa*) and two

*Corresponding author: Saleh M. Bufarwa, Chemistry Department, Omar Al-Mukhtar University, El-Beida City, Libya,

E-mail: saleh.bufarwa@omu.edu.ly. https://orcid.org/0000-0002-0869-2879

Reem M. El-Sefait and Rema. M. Abdusamea, Natural Resources and Environmental Sciences, Omar Al-Mukhtar University, El-Beida City, Libya, E-mail: Reem.elseifat@omu.edu.ly (R.M. El-Sefait),

rema.mohammed@omu.edu.ly (R.M. Abdusamea). https://orcid.org/0009-0006-2126-8278 (R.M. El-Sefait). https://orcid.org/0009-0000-3595-8241 (R.M. Abdusamea)

Dalal K. Thbayh, Institute of Chemistry, University of Miskolc, 3515 Miskolc-Egyetemváros, Hungary; Polymer Research Center, University of Basrah, Basrah, Iraq; and Higher Education and Industrial Cooperation Centre, University of Miskolc, 3515 Miskolc-Egyetemváros, Hungary, E-mail: dalal.thebayh@uobasrah.edu.iq. https://orcid.org/0000-0001-7938-2934

Mustapha Belaidi, Chemistry, Laboratory Environment and Sustainable Development Department, Ahmed Zabana University, 48000, Relizane Algeria; and Laboratory of Process Engineering and Environment, University of Sciences and Technologies of Oran (USTO), BP 1503, 31000 Oran, Algeria, E-mail: mustapha.belaidi@univ-relizane.dz. https://orcid.org/0009-0001-2483-4814

Rehab K. Al-Shemary, Chemistry Department, Baghdad University, Baghdad City, Iraq, E-mail: rehab.k.r@ihcoedu.uobaghdad.edu.iq. https://orcid.org/0000-0001-6865-7226

Marei M. El-Ajaily, Chemistry Department, Benghazi University, Benghazi City, Libya, E-mail: melajaily@gmail.com. https://orcid.org/0000-0001-9906-4554

Béla Fiser, Institute of Chemistry, University of Miskolc, 3515 Miskolc-Egyetemváros, Hungary; Department of Physical Chemistry, Faculty of Chemistry, University of Lodz, 90-236 Lodz, Poland; and Ferenc Rákóczi II Transcarpathian Hungarian College of Higher Education, Transcarpathia, 90200 Berezszáz, Ukraine, E-mail: bela.fiser@unimiskolc.hu. https://orcid.org/0000-0003-0603-4626

Hanan A. Bader, Chemistry Department, Omar Al-Mukhtar University, El-Beida City, Libya, E-mail: hanan.abdraba@omu.edu.ly. https://orcid.org/0009-0000-8520-9484

Abdulsalam A. Saleh, Perventive Medicine and Public Health Department, Omar Al-Mukhtar University, El-Beida City, Libya,

E-mail: abdulsalam.abdullah@omu.edu.ly. https://orcid.org/0009-0000-8193-9105

Mohamad M. Bufarwa, College of Education, Omar Al University, El-Beida City, Libya, E-mail: mohamad.momin@omu.edu.ly. https://orcid.org/0009-0002-3056-6980

fungal strains (Aspergillus flavus and Candida albicans) were tested and compared to the results of some standard drugs. The results revealed that compound C4 was more effective against bacterial strains than the comparison standard drugs. In addition, C3 was found to be the most effective of the comparison antibiotics against fungi, while the other compounds showed moderate antifungal activity. Moreover, to support the vitro results, certain computational studies as molecular docking studies, DFT, MESP, and AMEDT were also conducted to confirm the effectiveness of an organic ligand and its complexes against tuberculosis. These studies revealed that C4 is the most effective against tuberculosis and has desirable effects such as absorption, no degradation and no hepatotoxicity, etc.

Keywords: Schiff base; antituberculosis activity; anti-inflammatory activity; antimicrobial activity; molecular docking

1 Introduction

Although the use of antibiotics has improved public health around the world, inappropriate antibiotic usage has resulted in the emergence of bacteria that are increasingly resistant to most antibiotics, which means the fight against bacterial infections continues.³ From this vantage point, the fact that bacterial resistance is a concern everywhere on the globe has made it a major study focus.⁴ For instance, it has been discovered that the methicillin-resistant Staphylococcus aureus and the vancomycin-resistant Enterococcus are resistant to both drugs.⁵ The emergence of antibiotic-resistant bacteria and the limited efficacy of current antibiotics have made alternative strategies for combating bacterial infections essential to maintaining public health.⁶ A recent report by the World Health Organization (WHO) highlights tuberculosis infection (TB) as one of the leading causes of death worldwide. This infection is caused by a group of bacteria known as Mycobacterium tuberculosis. Shockingly, it has been found that around one person out of three is exposed to latent tuberculosis, which is capable of becoming active tuberculosis. 9 Tuberculosis is a disease that can spread among both humans and animals, including bovine tuberculosis, which is common in developing countries. 10 It is a chronic and infectious disease that affects livestock, wild animals, and humans alike, making it a significant public health concern. 11 Since their first synthesis by Hugo Schiff in 1864, Schiff bases have played a significant role in the development of chemistry. 12,13 When one equivalent of a diamine derivative is reacted with two equivalents of a salicylaldehyde derivative, a specific type of Schiff base called Salen is formed.¹³ The stability of salen complexes containing transition elements has made them a subject of numerous chemistry, physics, and medicine studies. Salen compounds act as tetradentate chelating ligands that form solid metal complexes. 14 The metal ion coordinates through four coordination sites, comprising three chelating rings with two oxygen and two nitrogen atoms. 15 Moreover. many studies have identified that Schiff base complexes of transition metals exhibit biological effects such as antibacterial, 16 antifungal, 17 anti-inflammatory, 18 antioxidant, 19 and anti-tumor activities.²⁰ Cytotoxicity data revealed that these exhibit significant non-toxic behavior, leading to the conclusion that they can be safely used as anti-inflammatory and anti-cancer agents.²⁰ Phenazines are a significant group of natural substances that are found in nature. They are crucial for medicinal purposes because of their excellent healing properties.²¹ Over the last century, scientists have discovered more than 6,000 phenazine-based compounds, and this number is constantly increasing due to their clinical effectiveness.²² One specific phenazine-based compound of great interest to chemists and biochemists is 2,3-diaminophenazine, which is an interesting aromatic compound possessing high electron density.²³ Some phenazine derivatives have been reported as antituberculosis agents, such as turbomycin and clofazimine, which have high activity against *M. tuberculosis*, in addition to their analogs, such as clofazimine with a C2-pyridyl substituent.^{22,24} So, during the search for an effective anti-infective agent, Schiff base compounds containing diaminophenazine moiety were synthesized due to their biological significance. Schiff base was synthesized by condensing two equivalents of 4-diethylaminosalicylaldehyde with 2,3-diaminophenazine to form 6,6'-((1E-1'E)(phenazine-2,3-dielbis(azanylidene)bis-(methanylidene)bis(3-(diethylamino)phenol) in methanol, which was further treated with Co(II), Ni(II), Cu(II) and Cd(II) nitrate to form the four complexes. The organic ligand and its complexes underwent characterization using various physical and spectroscopic techniques, including molar conductivity, melting point, magnetic susceptibility measurement, thermogravimetric analysis (TGA), elemental analysis (CHN), atomic absorption spectroscopy (AAS), nuclear magnetic resonance (¹H and ¹³C NMR), Fourier transform infrared (FT-IR), UV-Visible absorption (UV-Vis), electronic spin resonance (ESR) and mass spectra. Furthermore, the synthesized compounds were assessed for their antituberculosis, antibacterial, antifungal, antioxidant, anti-inflammatory, and cytotoxic activity and compared to standard drugs. To validate and support the present research, various computational studies were performed. These studies included an examination of the partial docking of compounds as well as the effects of absorption by absorption, distribution, metabolism, extraction, and toxicity (ADMET). Also, highlighted calculations of energy levels (HOMO and LUMO) and electronic distribution, as well as lengths of bonds and angles through discrete Fourier transform (DFT) studies.

2 Experimental

2.1 Chemicals

To conduct the current research, high-purity analytical reagents were used in the experiments including the following chemicals: 4-diethylaminosalicylaldehyde (98-%, Aldrich), 2,3-diaminophenazine (90 %, Aldrich), cobalt nitrate hexahydrate (98 %, Fluka), nickel nitrate hexahydrate (98.5 %, Fluka), copper nitrate trihydrate (99 %, Aldrich), cadmium nitrate tetrahydrate (98 %, Aldrich), dimethyl sulfoxide (99 %, Ficher), *N*,*N*-dimethyl formamide (99.9 %, Merck), methanol anhydrous (99.8 %, Aldrich), and ethanol (99.8 %, Fluka).

2.2 Apparatus

Molar conductivity measurements were obtained for solid compounds in dimethylformaldehyde (DMF) solution at room temperature by Jenway 4510 conductivity meter. Magnetic susceptibility calculations were performed using the Faraday method (Faraday equilibrium) at room temperature. The Perkin-Elmer 2400 CHN was utilized for elemental analysis. Also, the metallic content was determined using a Thermo Scientific iCE 3300 spectrometer atomic absorption spectrometer with an auto-sampler model. The FT-IR spectra were recorded using a Thermo Scientific 6700 and a KBr disc. The Beckman Coulter DU 800 spectrometer was used to obtain electronic spectra and dimethylsulfoxide (DMSO) as solvent. The mass spectra of compounds were performed by a direct input unit (DI-50) with the Shimadzu QP-5050 GC-MS. The ¹H and ¹³C NMR spectra were recorded using a Bruker high-performance Avance III NMR spectrometer at 400 MHz, with DMSO- d_6 as the solvent. The ESR spectra of the powder complexes were recorded at room temperature using a Jeol JES-FE 2XG spectrometer. Most of the analyses were carried out by the microanalysis team located at Cairo University in Giza, Egypt. To determine the antimicrobial and antioxidant activity, biological tests were conducted at the Department of Microbiology at Omar Al-Mukhtar University. Cytotoxicity and anti-tuberculosis activity were evaluated at the Faculty of Veterinary Medicine in collaboration with the Animal Health Center in the Laboratory of Preventive Medicine and Public Health.

2.3 Synthesis of ligand

The Schiff base ligand was prepared by 4-diethylaminosalicyaldehyde (1.93 g, 10 mmol) was added to $25\,\mathrm{mL}$ of hot methanol, followed by the addition of 2,3-diaminophenazine (1.05 g, 5 mmol) dissolved in $25\,\mathrm{mL}$ of methanol (Figure 1). 13,15 The mixture was heated and refluxed at 90 °C for 3 h. After condensation, the mixture was left to cool down to room temperature, resulting in the formation of orange precipitated crystals. The crystals were then isolated by filtration.

Characterization of 6,6'-((1E-1'E)-(phenazine-2,3-diylbis-(azanylylidene))bis-(metha-nylylidene))bis(3-(diethylamino) phenol) (H₂L): color: orange; yield: 70 %; m.p.: 132 °C; elemental analysis for organic ligand, m.wt: 560.702 g mol⁻¹ (C₃₄H₃₆N₆O₂) calculated: C, 72.83 %; H, 6.47 %; N, 14.99 %; found: C, 72.80 %; H, 6.40 %; N, 5.05 %. FT-IR (KBr, cm⁻¹): 3,047 ν (C–H)_{arm}; 3,359 ν (O–H); 1,244 ν (C–N)_{phe}; 1,610 ν (C=N)_{azo}; 1,025 ν (C–O). ¹H NMR (300 MHz, DMSO- d_6) δ 13.46 (m, 1H, OH), δ 13.36 (m, 1H, OH), δ 8.62 (m, 2H, CH=N), δ 8.52 (dd, J = 6.2, 3.4 Hz, 2H, Ar-H), δ 8.34 (s, 4H, Ar-H), δ 7.73 (dd, I = 6.2, 3.3 Hz, 2H, Ar-H), δ 7.38 (d, J = 2.1 Hz, 1H, Ar-H), δ 7.30 (d, J = 8.9 Hz, 1H, Ar-H), δ 7.09 (dd, J = 8.7, 2.2 Hz, 2H, Ar-H), δ 6.89 (J = 8.7, 2.5 Hz, 2H, Ar-H), δ 4.79 (q, J = 6.9 Hz, 4H, CH₂), δ 2.49 (t, J = 7.1 Hz, 6H, CH₃). ¹³C NMR (125 MHz, CDCl₃) δ 187.16, 183.09, 175.56, 169.66, 168.65, 168.01, 157.51, 156.52, 150.17, 149.16, 148.98, 146.03, 144.00, 71.80, 39.52.

2.4 Synthesis of complexes: a general produce

The complexes were prepared by mixing: $Co(NO_3)_2$ · $6H_2O$ (1.456 g, 5 mmol); $Ni(NO_3)_2$ · $6H_2O$ (1.454 g, 5 mmol); $Cu(NO_3)_2$ · $Cu(NO_3)_2$ ·C

Figure 1: Synthesis of 2,3-diaminophenazine Schiff base (**H**₂**L**).

2H₂O (1.208 g, 5 mmol) and Cd(NO₃)₂·4H₂O (1.542 g, 5 mmol) with the (2.803 g, 5 mmol) of organic ligand H₂L (molar ratio 1:1) in solvent mixture DMF/EtOH/H₂O (volume ratio 10:3:3 cm³). ¹⁵ The mixture was returned at 90 °C for 24 h, the prepared complexes were left to cool at room temperature. then the crystals were filtered. Different analytical methods were used characterize the ligand and its complexes with metal ions. The results obtained for the metal complexes were listed and summarized as follows:

2.4.1 Complex Co(II)L (C1)

Yield 72 %, color: dark wine, m.p.: 192 °C, m.wt: 617.21 g mol⁻¹, $\Lambda_{\rm m}$: 17.9 Ω^{-1} cm⁻¹ mol⁻¹; elemental analysis for complex (C₃₄H₃₄CoN₆O₂) calculated: C, 66.12 %; H, 5.55 %; N, 13.61 % and M, 9.54 %; found: C, 66.05 %; H, 5.52 %, N, 13.59 % and M, 9.57 %. FT-IR (KBr, cm⁻¹): 3,056 ν (C–H)_{arm}; 1,247 ν (C–O); 1,618 ν (C=N); 443 ν (Co-N); 525 ν (Co-O).

2.4.2 Complex Ni(II)L (C2)

Yield 73 %, color: orange, m.p.: 184 °C, m.wt: 617.37 g mol⁻¹, $\Lambda_{\rm m}$:17.4 Ω^{-1} cm⁻¹ mol⁻¹; elemental analysis for complex (C₃₄H₃₄NiN₆O₂) calculated: C, 66.12 %; H, 5.55 %; N, 13.61 % and M, 9.51 %; found: C, 66.11 %; H, 5.49 %, N, 13.68 % and M, 9.48 %. FT-IR (KBr, cm⁻¹): 3,047 ν (C–H)_{arm}; 1,258 ν (C–O); 1,618 ν (C=N); 441 ν (Ni–N); 526 ν (Ni–O).

2.4.3 Complex Cu(II)L (C3)

Yield 73 %, color: dark brown, m.p: 188 °C, m.wt: 622.23 g mol⁻¹, $\Lambda_{\rm m}$: 16.8 Ω^{-1} cm⁻¹ mol⁻¹; elemental analysis for complex (C₃₄H₃₄CuN₆O₂) calculated: C, 65.63 %; H, 5.51 %; N, 13.51 % and M, 10.21 %; found: C, 50.95 %; H, 5.54 %, N, 13.49 % and M, 10.18 %. FT-IR (KBr, cm⁻¹): 3,059 ν (C–H)_{arm}; 1,244 ν (C-O); 1,619 ν (C=N); 443 ν (Cu-N); 523 ν (Cu-O).

2.4.4 Complex Cd(II)L (C4)

Yield 78%, color: dark orange, m.p: 266°C, m.wt: 671.08 g mol⁻¹, $\Lambda_{\rm m}$: 18.5 Ω^{-1} cm⁻¹ mol⁻¹; elemental analysis for complex (C₃₄H₃₄CdN₆O₂) calculated: C, 60.85 %; H, 5.11 %; N, 12.52 % and M, 16.75 %; found: C, 61.05 %; H, 5.07 %, N, 12.48 % and M, 16.83 %. FT-IR (KBr, cm⁻¹): 3,053 ν (C–H)_{arm}; 1,245 ν (C–O); 1,620 ν (C=N); 428 ν (Cd–N); 574 ν (Cd–O). ¹H NMR (300 MHz, DMSO- d_6) δ 8.72 (m, 2H, CH=N), δ 8.45 (dd, J = 6.2, 3.4 Hz, 2H, Ar–H), δ 8.29 (s, 4H, Ar–H), δ 7.70 (dd, J = 6.2, 3.3 Hz, 2H, Ar-H), δ 7.37 (d, J = 2.1 Hz, 1H, Ar-H), δ 7.28 (d, J = 8.9 Hz, 1H, Ar-H), δ 7.01 (dd, J = 8.7, 2.2 Hz, 2H, Ar-H), δ 6.85 (J = 8.7, 2.5 Hz, 2H, Ar-H), δ 4.79 (q, J = 6.9 Hz, 4H, CH₂), δ 2.49 $(t, J = 7.1 \text{ Hz}, 6H, CH_3)$. ¹³C NMR (125 MHz, CDCl₃) 177.93, 172.58,

169.34, 168.81, 159.58, 157.21, 150.43, 149.87, 149.05, 146.63, 144.27, 71.96, 42.74.

2.5 Antimicrobial activity

In order to evaluate the antimicrobial activity of the ligand and its complexes, the agar-well diffusion method was used to test compounds and compare the efficacy with tetracycline, ciprofloxacin, and amphotericin B as standard drugs. 12,13 For the objective of comparison, the standard drugs and complexes were subject to identical concentrations and conditions. The antimicrobial activity of the complexes was subsequently assessed in vitro against two kinds of fungal: A. flavus and C. albicans strains as well as four bacterial strains: B. subtilis, S. aureus (+Gram), E. coli, and P. aeruginosa (-Gram).

2.6 Antioxidant activity

The assay measured the radical scavenging effect of stabilized 2,2-diphenyl-1-picrylhydrazyl (DPPH). 13 The 1 µg of ligand and its complexes were dissolved in 1 mL of DMSO, and their antioxidant activities were compared to ascorbic acid. 250 µL of each solution was added to 1 mL of DMSO/DPPH solution, which was prepared by dissolving 6 mg DPPH in 50 mL DMSO. The total volume was then adjusted to 3 mL by adding DMSO. The mixtures were incubated for 30 min at room temperature. The absorbance was measured at 517 nm wavelength. and the blank sample containing 3 mL of DMSO and DPPH was measured as well. The measurements were done in triplicate, and the value of radical scavenging activity was calculated using the following equation:

% reduction scavenging activity

$$= [A_{\text{control}} - A_{\text{sample}} / A_{\text{control}}] \times 100$$

Where: $A_{control}$: DPPH absorbance of radical + DMSO after 30 min.

 A_{sample} : DPPH absorbance + sample after 30 min.

$$AE = 1/IC_{50}$$

Where: AE: antiradical efficiency.

IC₅₀: concentration that had 50 % inhibition.

2.7 Cytotoxicity assay

The cytotoxicity assay was conducted using brine shrimp larvae, according to the protocol developed by Mayer et al.²⁵ This method has been found to correlate well with cytotoxic activity, while it is also cost-effective. Shrimp eggs were incubated in a rectangular dish filled with seawater with the help of the Department of Preventive Medicine and Public Health Laboratory at Omar Al-Mukhtar University. To create an uneven section in the plate, a perforated tool was used. About 50 mg of eggs were sprayed into a large dark chamber, while the smaller chamber was exposed to normal light. After two days, the larvae were collected in a pipette with a lighted side. To perform the test, stock solutions of each test compound were prepared by dissolving 10 mg of the compound in 10 mL of DMSO. Different concentrations of compounds were added to separate vials and the final volume was adjusted to 10 mL with seawater after two days. Once the shrimp larvae were ready, we added 10 larvae to each vial and incubated them for 24 h. The vials were then observed using a magnifying glass and the number of surviving individuals in each vial was counted. The test was performed in duplicate and Finney computer software was used to analyses the data and determine the LD_{50} . The results were compared with a control group positive for the anticancer drug bleomycin.

2.8 Anti-inflammatory activity

The anti-inflammatory activity of the organic ligand and its complexes was evaluated using a BSA (bovine serum albumin, 98 %, Aldrich),) assay.²⁶ The test was conducted in triplicate with aspirin and sodium diclofenac as standard drugs. Compounds were prepared in DMSO with dilute phosphate buffer (0.2 M, pH 7.4) at concentrations of 15, 25, 50, 100, and 200 μ g L⁻¹. 1 mL of BSA (1 mM) in phosphate buffer was dissolved in 4 mL containing various concentrations of the compounds. The BSA was denatured in a water bath at 70 °C for 15 min after incubating the solutions at 37 °C for 20 min. After allowing the solutions to cool at ambient temperature, the test solutions exhibited turbidity. Finally, the absorbance was measured at 660 nm using a UV-Vis spectrometer, and the % denaturation was determined as a control in the absence of any drug and the inhibition of BSA was assessed using the following formula:

% BSA inhibition = $(1 - X)/Y \times 100$

Where: *X*: absorbance of the control. Y: absorbance of the compounds.

2.9 Anti-tritubercular activity

All compounds were evaluated in vitro for anti-TB using the proportion method.²⁷ To perform this method, a Lowenstein-Jensen (LJ) medium was prepared by mixing fresh chicken eggs with mineral salt and adding 2 % malachite

green. A stock solution of the test compound was created in DMF and then filtered through a 1 µg porous membrane. It was then diluted to 1, 2 and 3 µg/mL. Each solution was transferred to a sterile universal container and put in isolation at 85 °C for 45 min. Control experiments were also conducted without the presence of the test compound. Mel (LI) was inoculated with 10⁻⁴ CFU mL⁻¹ of standard **M.TB** H_{37RV} and the clinical isolate. They were successively incubated at 37 °C for 28 days. The tested compounds were also incubated for 14 days and compared with pyrazinamide (PZA) as a standard.

2.10 Computational studies

The computational studies mentioned below were performed on the organic ligand and its metal complexes against active anti-tuberculosis compounds to support in vitro results.

2.10.1 Generation and optimization of compounds

The molecular editor Gauss View 6.0. was used to create and optimize the three-dimensional structure of the organic ligand and its metal complexes. To obtain the optimization of exchange and correlation functions, B3LYP was applied with basic set 6-31G (d,p)/LANL2DZ.

2.10.2 Obtaining the three-dimensional structure of the target

The target structure for pfndh was obtained from the Protein Data Bank (PDB) (www.rcsb.org) to serve as the intended

2.10.3 Molecular docking

The significance of molecular docking lies in its ability to predict the conformation of compounds within the active sites or the target molecular binding site, as well as to predict the binding aspects of a specific interaction. Using the AutoDock tool, 28,29 molecular docking was carried out on an organic ligand and its complexes with a specific target of the M. tuberculosis structure (PDB ID:1DQZ) obtained from the Protein Data Bank.

2.10.4 DFT and MESP analysis

Molecular properties and analysis of chemical reactions to predict the ability of compounds to interact with each other rely largely on theoretical methods. These methods are frequently used to determine the molecular structure of manufactured compounds because they are efficient and

accurate. Therefore, some theoretical studies were carried out to obtain additional information about the computer calculations of the prepared compounds. Related fields were also studied based on density functional theory (DFT).³⁰ Studying the relationship between the geometry and electronic properties of chemical compounds that contain the highest occupied molecular orbitals (HOMO) and lowest occupied molecular orbitals (LUMO) orbitals is crucial, along with some quantity parameters. In addition, the bond lengths and angles of the prepared compounds were calculated computationally.

2.10.5 ADMET analysis

The AdmetSAR web server was used to anticipate the absorption, metabolism, and carcinogenicity of the ligand and its metal complexes. To do this, the structures of the compounds were uploaded onto the server and the drug-like compounds were assessed based on their ADMET characteristics.³¹

3 Results and dissection

3.1 Chemistry

Metal ion complexes of Co(II), Ni(II), Cu(II) and Cd(II) were prepared in the solid state. They are soluble in some organic solvents, such as DMF and DMSO, and not soluble in water. The low molar conductivity of the complexes was measured in 10^{-3} M in DMF solution at ambient temperature, indicating that they are non-electrolyte in nature.³² The thermal stability of the complexes was determined up to 253 °C using TGA. The square planar geometry of the N and O atoms of the Schiff base ligand in the complexes was determined using various spectral analysis methods.

3.2 Spectral and physical methods

The current study, investigated the nature of chemical bonding between atoms, using thermal decomposition and various spectral and physical techniques for analysis, as shown below.

3.3 Elemental analysis

The elemental components and the purity of the prepared complexes were determined by (C %, H %, N % and M %) elemental analysis and are mentioned in (Table 1).

3.4 Molar conductivity

The molar conductivity of the prepared complexes was measured using a 10⁻³ M dimethylformamide (DMF) solution. The obtained results showed that the C1, C2, C3, and C4 complexes have low molar conductivity values (17.9, 17.4, 16.8, and $18.5 \,\Omega^{-1} \,\mathrm{cm}^2 \,\mathrm{mol}^{-1}$). These values confirmed that the complexes are non-electrolytic in nature.³²

3.5 Mass spectra

The peaks of the complexes' mass spectra were recorded by correlating the peaks of the molecular ions (m/z) with the molecular mass of the complexes. The bonds of the complexes show molecular ionic peaks at m/z 617.2, 616.2, 621.2, and 672.1 for C1, C2, C3, and C4, respectively, which is consistent with the proposed molecular mass values for complexes (Figures S1-S4).

3.6 FT-IR spectra

Table 2 presents the FT-IR data for the ligand and their corresponding metal complexes. In the FT-IR spectra, the free Schiff base ligand H2L displays a sharp band at 1,630 cm⁻¹, which is attributed to the ν (C=N) azomethine group. 14 Additionally, the broadband at 3,359 cm⁻¹ indicates the presence of the $\nu(OH)$ phenolic group in the ligand. ^{23,33} Furthermore, the range of 1,237 cm⁻¹ shows the occurrence of $\nu(C-O)$ phenolic. The broadband is observed in regions 1,547 and 1,258 cm $^{-1}$ due to the (C=C) and (C-N), respectively.³⁴ Upon chelating, the bands are shifted higher or lower indicating the participation of the phenolic oxygen atom in coordination with the metal ion. Based on the non-electrolytic nature of metal complexes, it can be concluded that metal ions coordinate with phenolic oxygen due to their bivalency satisfaction.³⁵ The absence of broadband attributed to $\nu(OH)$ phenolic in the FT-IR spectra of metal complexes indicates the coordination of the central metal bonds of C1, C2, C3, and C4 by the phenolic oxygen atom.³⁶ This shift is attributed to the decrease in the property of the double bond between ν (C=N) azomethine, which occurred due to the entry of nitrogen into coordination with the metal ion.³⁷ The ν (M–O) and ν (M–N) complexes have frequency patterns of 525, 526, 523, and 541 cm⁻¹; and 443, 441, 443 and 487 cm⁻¹, respectively. 38,39

Table 1: Physical features of ligand (HL) along with its complexes.

Symbol	Molecular formula	M wt	Color	Yield %	Λ _m	M.p. °C		Cal (fo	ound) %	
						С	С	Н	N	М
HL	C ₃₄ H ₃₆ N ₆ O ₂	560.69	Orange	70	-	132	72.83	6.47	14.99	_
							(72.80)	(6.40)	(15.05)	-
C1	$C_{34}H_{34}N_6NiO_2$	617.37	Orange	73	17.9	184	66.15	5.55	13.61	9.51
							(66.04)	(5.49)	(13.57)	(9.48)
C2	$C_{34}H_{34}CoN_6O_2$	617.21	Dark wine	72	17.4	192	66.12	5.55	13.61	9.54
							(66.05)	(5.52)	(13.59)	(9.57)
C3	$C_{34}H_{34}CuN_6O_2$	622.22	Dark brown	74	16.8	188	65.63	5.51	13.51	10.21
							(65.60)	(5.48)	(13.46)	(10.25)
C4	$C_{34}H_{34}CdN_6O_2$	671.08	Dark orange	73	18.5	266	60.85	5.11	12.52	16.75
							(60.93)	(4.98)	(12.60)	(16.80)

 Table 2: FT-IR spectra characterization of organic ligand and its complexes.

Compound	ν(OH) _{phenolic}	ν(C=C) _{aromatic}	ν(C=N) _{azomethine}	ν(C-O) _{phenolic}	ν(MN)	ν(MO)
H ₂ L	3,359	1,574	1,630	1,237	-	_
C1	_	1,557	1,594	1,188	443	525
C2	_	1,561	1,581	1,207	441	526
C3	_	1,556	1,589	1,194	443	523
C4	-	1,559	1,615	1,175	487	541

3.7 Electronic absorption spectra and magnetic moments

The stereochemistry of the organic ligand H2L and its complexes is well examined by UV-Vis spectra, which were evaluated in DMSO at ambient temperature (Figure S6). The absorption band recorded at (273 nm. 36,630 cm⁻¹) was assigned to $\pi \rightarrow \pi^*$ transitions that correspond to the phenolic ring of the ligand. 40 The absorption band at (406 nm, 24.630 cm⁻¹) is attributed to $n\rightarrow \pi$ transitions of azomethine. 41 compared with the organic ligand, the Co(II) and Ni(II) complexes showed three absorption bands, while the Cu(II) complex contained two absorption bands, while the Cd(II) complex showed one absorption band due to the d¹⁰ electronic configuration and charge transfer from the ligand to the Cd(II) ion and are mentioned in (Table 3).⁴² Magnetic moment values for C1, C2, and C3 complexes were found in the range of 2.1, 1.6, and 1.5 BM, respectively, and the C4 complex did not show a value for the magnetic moment due to the electrical configuration of d10.43

3.8 1 H NMR and 13 C NMR spectra

¹H and ¹³C NMR analysis provides the positions of proton and carbon signals for the Schiff base ligand H2L and its C4 (Table 4, Figures S7 and S8). Two phenol δ OH signals were observed at 13.43 and 13.46 ppm, while the δ CH=N signal of the azomethine proton appeared at 8.62 ppm in the ¹H NMR spectra of the ligand.²³ Fourteen aromatic δ C–H protons were recorded in the range of 4.79 ppm, and there were four aliphatic δ CH₂ protons and six δ CH₃ protons in the ligand.⁴⁴ In the **C4**, the phenol proton at δ OH 13.43 and 13.46 ppm in the ligand disappears due to its entry into the complex.¹³ Moreover, the signal shift of the azomethine group of the ligand indicates the formation of the complex via the nitrogen atom of azomethine. In the ¹³C NMR spectra, a signal appears at 187.16 ppm attributed to two azomethine carbons in the ligand. Signals also appear at 175.56-144.00 ppm are attributed to the carbons in the aromatic ring of quinoxaline, C27, C28, C29, C30, C31, C32, C33, C35, C37, C38, C39, C40 and C41. The signal for the aliphatic CH₃ group appears at 39.52 ppm, C11, C12, C25 and C26, while the aliphatic CH₂ signal appears at 71.80 ppm, C10, C11, C23 and C24.42

Table 3: Electronic spectra data of ligand and its complexes.

Compound	λ (nm) and υ (cm ⁻¹)	Band assignments	μ _{eff} (BM)	Suggested structure
H ₂ L	273 nm,	π→π* benzene	-	-
	36,630 cm ⁻¹	ring		
	406 nm,	$n{\to}\pi^{\textstyle\star}$ azomethine		
	24,630 cm ⁻¹			
C1	257 nm,	HL chromophore	2.1	Square planar
	38,910 cm ⁻¹	(π→π *)		
	387 nm,	` '		
		$^{4}T_{1g}(F) \rightarrow ^{4}T_{1g}(P)$		
		$^{4}\text{T}_{1g}(\text{F}) \rightarrow ^{4}\text{A}_{2g}(\text{P})$		
	10,593 cm ⁻¹	, ,		
		$^{4}\text{T}_{1g}(\text{F}) \rightarrow ^{4}\text{T}_{2g}(\text{P})$		
	8,244 cm ⁻¹			
C2		HL chromophore	1.6	Square planar
	39,525 cm ⁻¹	` '		
		$(C.T)^{1}A_{1g} \rightarrow {}^{1}A_{2g}$		
	25,974 cm ⁻¹	2. 1-		
		$^{2}A_{1g} \rightarrow ^{1}E_{g}$		
	22,831 cm ⁻¹	1. 1.		
		$^{1}A_{1g} \rightarrow ^{1}A_{2g}$		
	16,181 cm ⁻¹			
C3		HL chromophore	1.5	Square planar
	39,215 cm ⁻¹	, ,		
		$(C.T)^{2}B_{1g}\rightarrow^{2}E_{g}$		
	26,595 cm ⁻¹	2p 24		
	580 nm, 17,241 cm ⁻¹	$^{2}B_{1g}\rightarrow^{2}A_{1g}$		
64	*		D:-	C
C4	284 nm, 35,211 cm ⁻¹	HL chromophore	Dia.	Square planar
	-	$(\Pi \rightarrow \Pi^*)$ (C.T) (L \rightarrow M)		
	380 nm, 26,315 cm ⁻¹	(C.1) (L→IVI)		
	20,515 CIII			

Table 4: 1 H NMR and 13 C NMR data in ppm of organic ligand and its Cd complexe.

Compound	¹ H NMR (DMSO- <i>d</i> ₆ – 300 MHZ)	¹³ C NMR (CDCl ₃)
H ₂ L	δ 13.43–13.46 (m, s, 2H for OH phenolic ring), δ 8.62 (d, J , 2H for CH=N azomethine), δ 6.89–8.53 (s, m, 14H, for C–H aromatic ring), 4.79 (m, 6H for C–H aliphatic)	δ 187.16, 183.09, 175.56, 169.66, 168.65, 168.01, 157.51, 156.52, 150.17, 149.16, 148.98, 146.03, 144.00, 71.80, 39.52
C4	δ 8.97 (d, J , 2H for CH=N azomethine), δ 7.47–8.15 (s, m, 14H, for C–H aromatic ring), 4.76 (m, 6H for C–H aliphatic)	δ 180.57, 170.38, 167.75, 162.83, 154.53, 154.47, 149.76, 149.16, 148.67, 145.94, 143.85, 70.92, 39.47

3.9 ESR spectra

ESR spectra of a metal complex provide information about the metal and its environment within the complex. 45 This

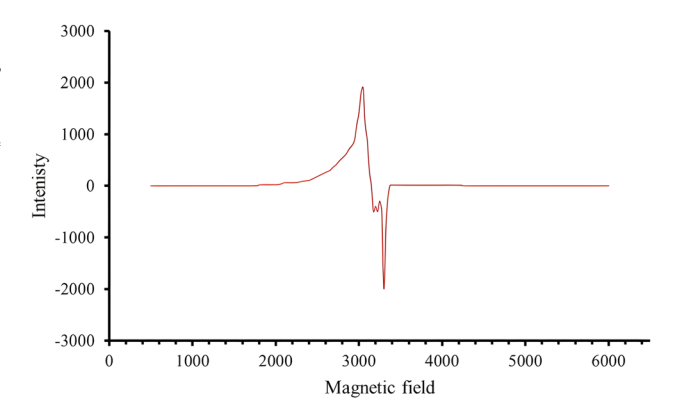


Figure 2: The ESR spectra of H_2L and C1, C2, C3 and C4 at room temperature.

includes details about the geometric structure and location arrangement of the Schiff base and the metal. Figure 2 illustrates the ESR spectra of the copper complex at room temperature. The data suggests that the delocalized electron is in the dx^2-y^2 orbital and its ground state is ${}^2B_{1g}$ with square planar geometry. The metal-ligand bonds have a covalent nature with a g_{\parallel} value of less than 2.0023. Hathaway's statement suggests that if G < 4, there are some exchange interactions, while if G > 4, there is little interaction between the copper ions. The properties of the square planar geometry can be determined by the symmetry axis parameter G, which has a value of 1.609, indicating significant exchange interactions between the copper centers. 46 Furthermore, the correlation parameters α^2 (in-plane σ bonding), β^2 (in-plane π bonding), and y^2 (out-plane π bonding), were predicted based on the values of the basic parameters derived $(g_{\parallel}, g_{\perp} \text{ and } A_{\parallel})$ as shown in Table 5. The resulting values indicate that $K_{2\parallel} > K_{2\perp}$, suggesting the presence of a large external bond in the copper complex, confirming its strong covalent nature.

3.10 Thermal analysis

In the current work, we conducted thermal analysis to investigate the thermal stability of Schiff base complexes, synthesized during the research. The aim was to determine the presence or absence of solvent molecules, and whether they were located inside or outside the inner coordination sphere of the complex. The ligand and its complexes underwent thermogravimetric analysis from 0 to 600 °C with a heating rate of 10 °C min⁻¹. All thermal decomposition data for the ligand and its complexes shown in (Figure 3) are listed in (Table 6). The thermal curve pattern for the decomposition of C1, C2, and C3 complexes converges in three steps, with a slight difference in C4, which has four steps. The complexes begin to decompose in the first step at a

Table 5: Spin Hamiltonian parameters of the copper complex at room temperature.

Complex	g_{\parallel}	g _ŵ	A_{\parallel}	α²	β²	γ²	<i>K</i> _{2∥}	K _{2�}	$\mu_{ m eff}$
C3	2.0757	2.0304	0.0187	0.650	0.196	0.302	0.127	0.046	1.5

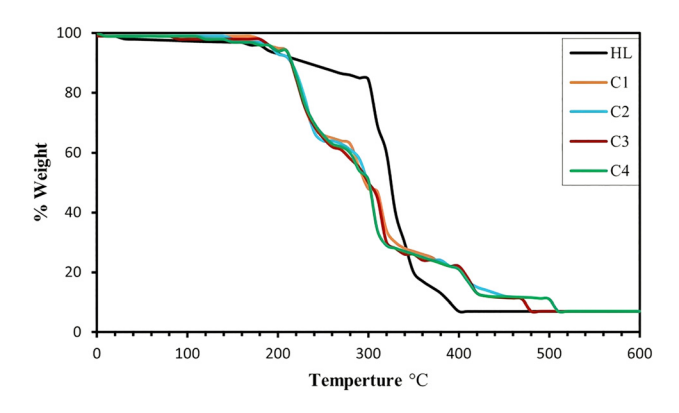


Figure 3: TGA curve of H₂L and C1, C2, C3 and C4.

temperature range at 218–243 °C with the loss of the two azomethine groups and part of the organic ligand. In the second step, the remaining organic ligand decomposes at 235–520 °C, leaving the metal oxide as a final product behind.

3.11 Geometrical structures

The geometries of ligand and the metal complexes were calculated after optimizing the angle and bond lengths using the Gaussian 09 program package. Density functional theory (DFT) method has been used, the B3LYP functional along with the 6-31G(d) basis set for ligands and LANL2DZ for metals in the solvent phase. Structure data for the selected bond lengths are listed in (Table 7 and 8). The optimized conformations of all complexes are listed in (Figure 4). Structure data for the selected bond lengths are listed in (Table S2). The bond lengths of all complexes of the optimized conformations in (Figure 11) are listed in (Tables S3–S4). The theoretical data showed several points:

 The lengths of bonds belonging to the coordinated atoms suffer elongation from the free ligand, due to the entry of MO and MN into coordination.

Table 6: Thermal analysis of the decomposition of metal complexes.

Symbol	Molecular formula (molecular weight)	TG range °C	% we	ight lost	Assignments
			Calc.	(Found)	
H ₂ L	C ₃₄ H ₃₆ N ₆ O ₂ (560.69)	170-400	12.84	(12.90)	- C ₄ H ₁₀ N
			87.03	(86.91)	$- C_{30}H_{27}N_5O_2$
C1	C ₃₄ H ₃₄ N ₆ CoO ₂ (617.21)	218-235	8.75	(8.69)	 Loss of two azomethine gro
	Residue	235-320	28.84	(28.79)	 Loss of phenazine group
		320-410	23.82	(23.80)	 Loss of diethylanline
		410-480	26.41	(26.40)	 Loss of diethylaminopheno
		>480			- CoO
C2	$C_{34}H_{34}N_6NiO_2$ (617.37)	220-240	8.75	(8.71)	 Loss of two azomethine gro
	Residue	240-325	28.83	(28.85)	 Loss of phenazine group
		325-420	23.81	(23.80)	 Loss of diethylanline
		420-487	26.40	(26.39)	 Loss of diethylaminopheno
		>487			- NiO
C3	C ₃₄ H ₃₄ N ₆ CuO ₂ (622.22)	220-239	8.68	(8.70)	 Loss of two azomethine gro
	Residue	239-296	28.61	(28.60)	 Loss of phenazine group
		296-386	23.63	(23.64)	 Loss of diethylanline
		386-494	26.20	(26.19)	 Loss of diethylaminopheno
		>494			- CuO
C4	C ₃₄ H ₃₄ N ₆ CdO ₂ (671.08)	219-243	8.05	(8.07)	 Loss of two azomethine gro
	Residue	243-320	26.52	(26.51)	 Loss of phenazine group
		320-410	21.90	(21.87)	 Loss of diethylanline
		410-480	10.89	(10.90)	 Loss diethylamine
		480-520	13.56	(13.58)	 Loss of phenol
		>520		, ,	- CdO

Table 7: The calculated quantum chemical parameters of complexes.

Complex	номо	LUMO	$\boldsymbol{\mathit{E}}_{g}$	χ	η	σ	Pi	S	ω	ΔΝ
C1	-5.07	-2.58	2.49	3.83	1.25	0.8	-3.83	0.4	5.87	3.06
C2	-5.13	-2.60	2.53	3.87	1.27	0.79	-3.87	0.39	5.88	3.04
C3	-5.11	-2.56	2.55	3.84	1.28	0.78	-3.84	0.39	5.76	3.01
C4										

Table 8: The selected angle length (Å) of complexes.

Bond	H ₂ L		Bond le	ngth (Å)	
		C1	C2	С3	C4
C1-O	1.36783	1.30922	1.30887	1.31157	1.30866
C2-O	1.36783	1.30924	1.30924	1.31157	1.30866
C3-N	1.29520	1.32137	1.32341	1.32486	1.31531
C4-N	1.29520	1.32130	1.32311	1.32488	1.31544
C5-N	1.39340	1.40142	1.40576	1.40673	1.39387
C6-N	1.39343	1.40137	1.40549	1.40672	1.39349
C7-N	1.34072	1.34261	1.34277	1.34281	1.34181
C8-N	1.34071	1.34261	1.34276	1.34281	1.34174
C9-N	1.35023	1.34797	1.34758	1.34712	1.34952
C10-N	1.35023	1.34796	1.34763	1.34712	1.34944
O1-M	-	1.94011	1.90472	1.86628	2.20046
O2-M	-	1.94144	1.90450	1.86618	2.20065
N1-M	-	1.99403	1.92699	1.89204	2.37506
N2-M	-	1.99495	1.92721	1.89196	2.37511

- The MN bond is longer than the MO bond in all complexes.
- There was no significant change in the other bond lengths of the atoms.

The two basic orbitals that play a crucial role in chemical stability are the highest molecular orbital, HOMO, and the unoccupied molecular orbital, LUMO. The HOMO refers to the ability to donate an electron, while LUMO refers to the ability to gain an electron as an electron acceptor. The (Table 9 and Figure 5) list the HOMO and LUMO energies obtained from calculations of complexes with C1, C2, and C3. Moreover, additional parameters such as HOMO-LUMO energy gap E_{g} , absolute electronegative χ , chemical potentials Pi, absolute hardness η , absolute softness σ , global electrophilicity ω , global softness S and additional electronic charge ΔN_{max} were calculated and are listed in (Table 9). 51,52 The energy gap $E_{\rm g}$. between HOMO and LUMO is an important metric for predicting the stability of compounds. A lower value of the energy gap E_g . indicates a higher reactivity of the compound.⁵² Compared to the other complexes, the C3 complex was found to be the most reactive. The energy gap values of the complexes C1, C2, C3, and C4 are 0.76, 0.73, 0.43, and 2.57 eV, respectively.

Understanding the polarizability, acid-base behavior, structural properties of a molecule, and electrophilic attack sites through electrostatic potentials is crucial and has various applications in quantum chemical calculations. Figure 5 demonstrates the significance of the MESP (Molecular Potential Surface) chart, which was introduced by Gauss View 6.0.1 in the chart, the red, green, and blue colors indicate the negative, neutral, and positive ESP (Electrostatic Potential) regions, respectively. Figure 6 depicts the most positive element of the Cd(II) atom. Generally, the highest negative ESP region is observed in the phenolic oxygen atoms, the two nitrogen atoms of the Schiff base, and the two nitrogen atoms of the phenazine moiety.

3.12 Biological activity

3.12.1 Antimicrobial activity

The antibacterial and antifungal activities of a ligand and its complexes were tested against six different microorganisms, including *B. subtilis, S. aureus, E. coli, P. aeruginosa, A. flavus*, and *C. albicans*. The tests were conducted using a DMSO solvent with a concentration of 1 mg mL⁻¹, and the well-diffusion method was employed to determine the results. The standard drugs Ciprofloxacin, Tetracycline, and Amphotericin B were also screened at the same concentration. The data presented in (Table 10 and Figure 7) demonstrate that the complexes exhibit moderate to good antibacterial activity as compared to standard drugs. The following points provide a summary of the obtained results:

- The ligand and its complexes were found to have only slight activity against *C. albicans*, except the C3 which showed more significant activity.
- The ligand and its complexes exhibited higher activity against bacterial strains and, in some cases, higher than the standard drugs tested. iii. In some cases, the data showed that activity increased after complexation compared to the free ligand.⁵³ This can be attributed to the chelation theory, which proposes that complexation reduces the polarity of the bond between the central

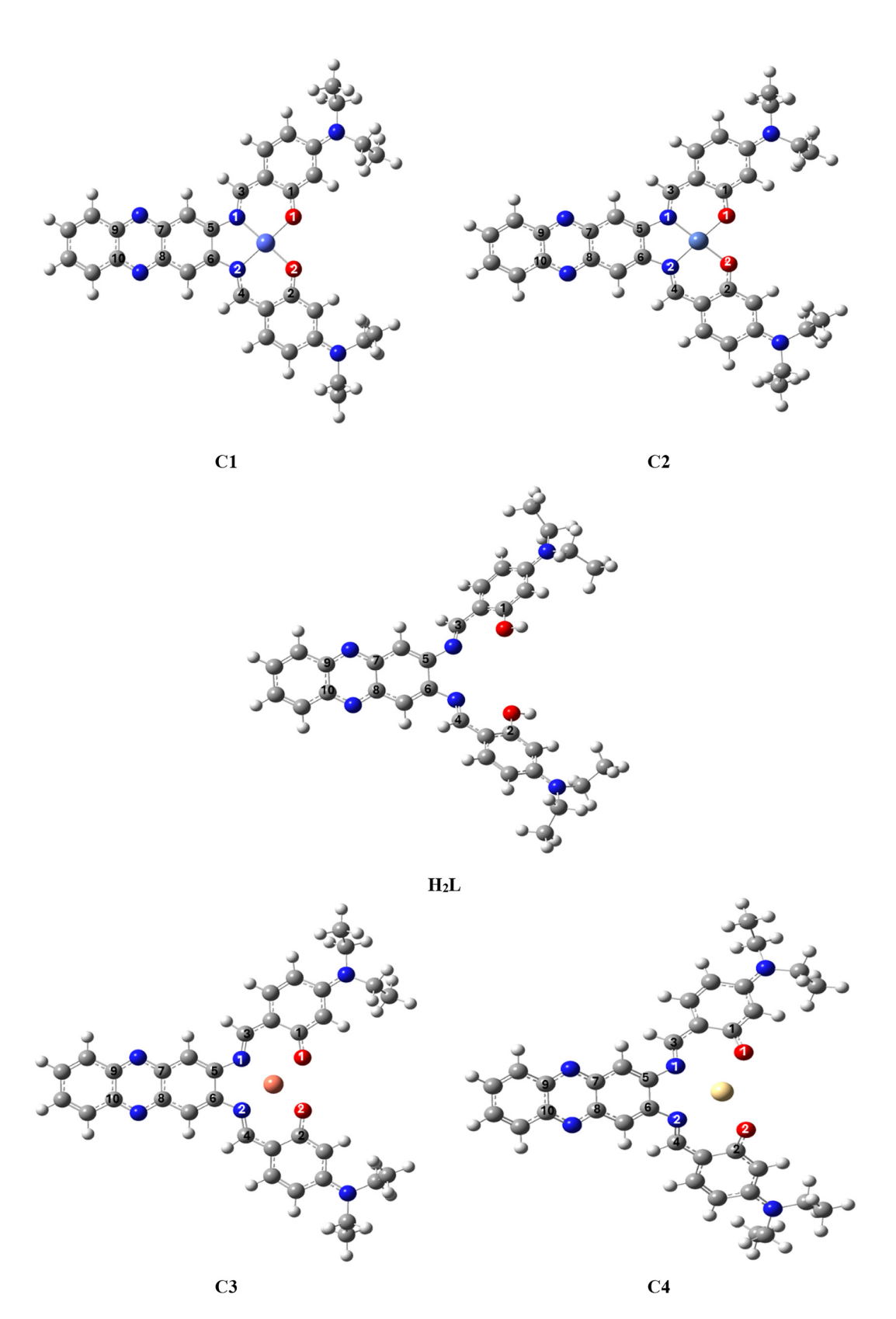


Figure 4: The optimized conformations of H_2L and C1, C2, C3 and C4.

Table 9: The selected bond length (Å) of complexes.

H ₂ L	Start atom	End atom	C1	Start atom	End atom	C2	Start atom	End atom	C3	Start atom	End atom	C4	Start atom	End atom
CNC 122.38	C21	N1	N-Co-N 86.25	N1	N2	N-Ni-N 86.84	N1	N2	N-Cu-N 87.52	N1	N2	N-Cd-N 86.99	N1	N2
CNH	C23	H35	N-Co-O 94.41	N1	01	N-Ni-N 94.40	N1	01	N-Cu-O 94.24	N1	01	N-Cd-O 93.57	N1	01
CNH	C23	H35	N-Co-O 179.41	N1	02	N-Ni-O 178.74	N1	02	N-Cu-O 176.26	N1	02	N-Cd-O 178.83	N1	02
CNC	C22	N2	N-Co-O 179.34	N2	02	N-Ni-O 178.74	N2	01	N-Cu-O 176.26	N2	01	N-Cd-O 178.83	N2	01
COH 123.83	C1	H37	O-Co-O 85.00	01	02	N-Ni-O 94.41	N2	02	O-Cu-O 83.81	N2	02	O-Cd-O 93.57	N2	02
COH 123.83	C7	H38	Co-NC 125.22	Со	C21	Ni-NC 126.19	Ni	C21	Cu-NC 125.57	Cu	C21	Cd-NC 124.86	Cd	C21
			Co-NC 125.29	Со	C23	Ni-NC 121.71	Ni	C23	Cu-NC 109.59	Cu	C23	Cd-NC 126.86	Cd	C23
			Co-OC 130.59	Со	C1	Ni-OC 133.91	Ni	C1	Cu-OC 132.04	Cu	C1	Cd-OC 131.15	Cd	C1
			Co-OC 130.67	Со	C7	Ni-OC 133.91	Ni	C7	Cu-OC 132.03	Cu	C7	Cd-OC 131.15	Cd	C7

atom and the ligand, making it easier for the complexes to penetrate the lipid layer of the cell membrane.⁵⁴

3.12.2 Antioxidant activity

The antioxidant activity of the ligand and its complexes was evaluated by comparing them with ascorbic acid, which was used as a standard. The DPPH assay results for the ligand and its complexes as shown in (Figure 8) indicated that they had higher antioxidant activity than the standard. The IC₅₀ values revealed that the ligand and its complexes exhibited antioxidant activity in the following order: $C3 > C2 > C1 > C4 > H_2L.$

3.12.3 Cytotoxicity assay

The brine shrimp cytotoxicity assay is a good tool for biomonitoring, used to determine the ability of cells to kill cancer cells.²⁰ The results of the cytotoxicity test for compound H2L and its compounds with metal(II) are summarized in (Table 11). Among all the compounds tested, the C4 and C2 compounds exhibited the highest cytotoxicity, with LD_{50} values of 1.157 \times 10⁻⁴ and 1.836 \times 10⁻⁴, respectively. On the other hand, the H₂L, C3, and C1 compounds were less effective against A. salina.

3.12.4 Anti-inflammatory activity

Inflammation can be caused by various factors such as temperature, external stress, and organic solvents, which can disrupt protein structure and lead to pathogenic diseases. Inflammation can be beneficial as a defense mechanism against tissue damage, but it can also contribute to serious illnesses such as asthma, arthritis, etc.(Table12 and Figure9)³⁰

- (1) The study showed that all compounds were highly effective in inhibiting inflammation, and the percentage of inhibition rate increased with the concentration, as shown in (Table 12). The anti-inflammatory activity of the ligand can be observed, which is comparable to its complexes with enhanced efficacy.
- (2) It has been observed that the complexes exhibit a trend of C4 > C3 > C2 > H_2L > C1 in terms of activity. This is due to the property of protein denaturation present in the complexes, which helps prevent the formation of adema and water retention and indicates a decrease in inflammation.⁵⁵ Other factors such as hydrophilicity, chelation, and metallic effects may also impact biological activity.⁵³
- From the data listed in (Table 12 and Figure 9), the results indicate that C4 complex is significantly active as an antiinflammatory with 34.74 % at 200 µg mL⁻¹, which can be compared with standard drugs.

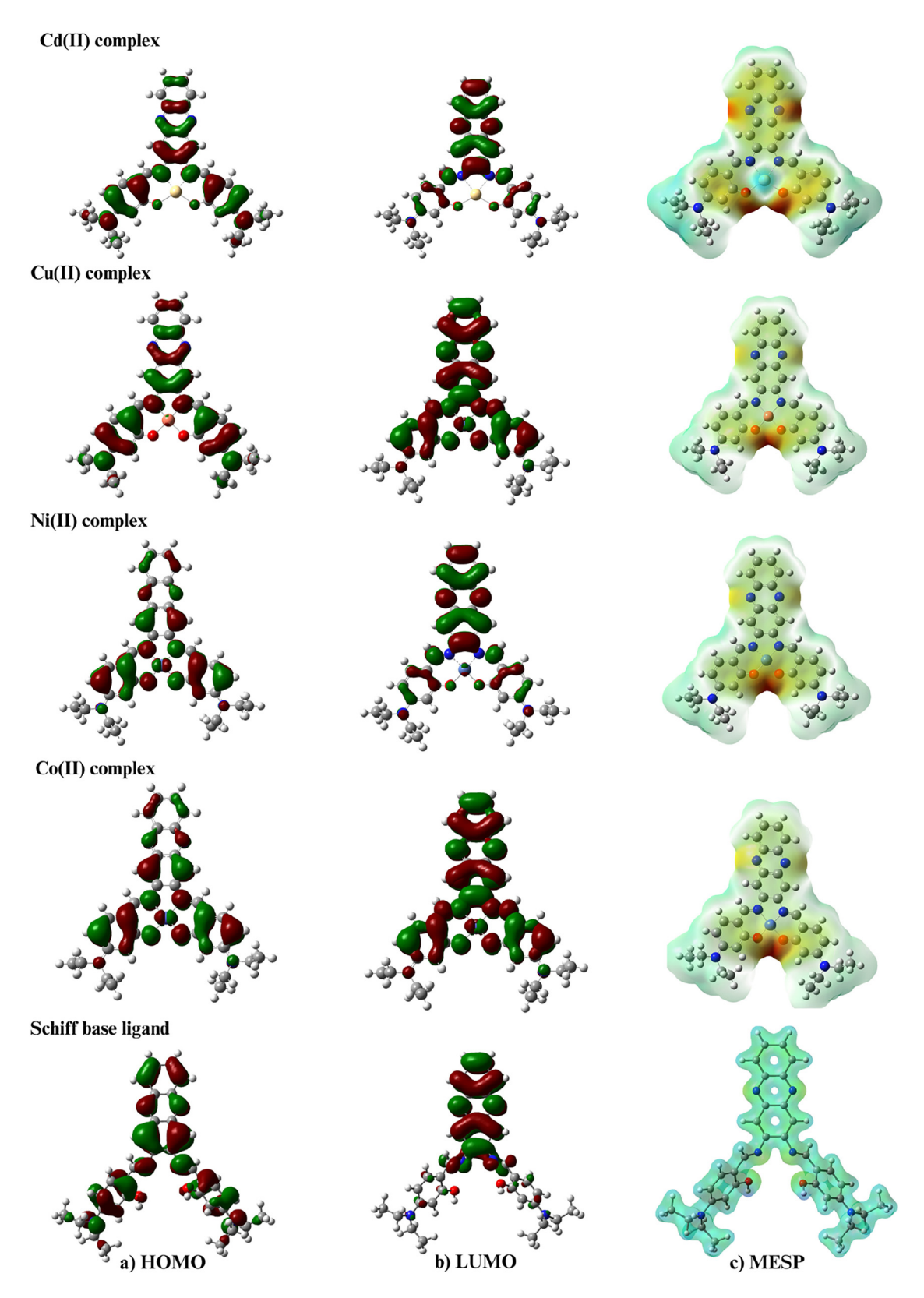


Figure 5: Molecular orbital distribution plots of HOMO, LUMO state, and MESP of the compounds.

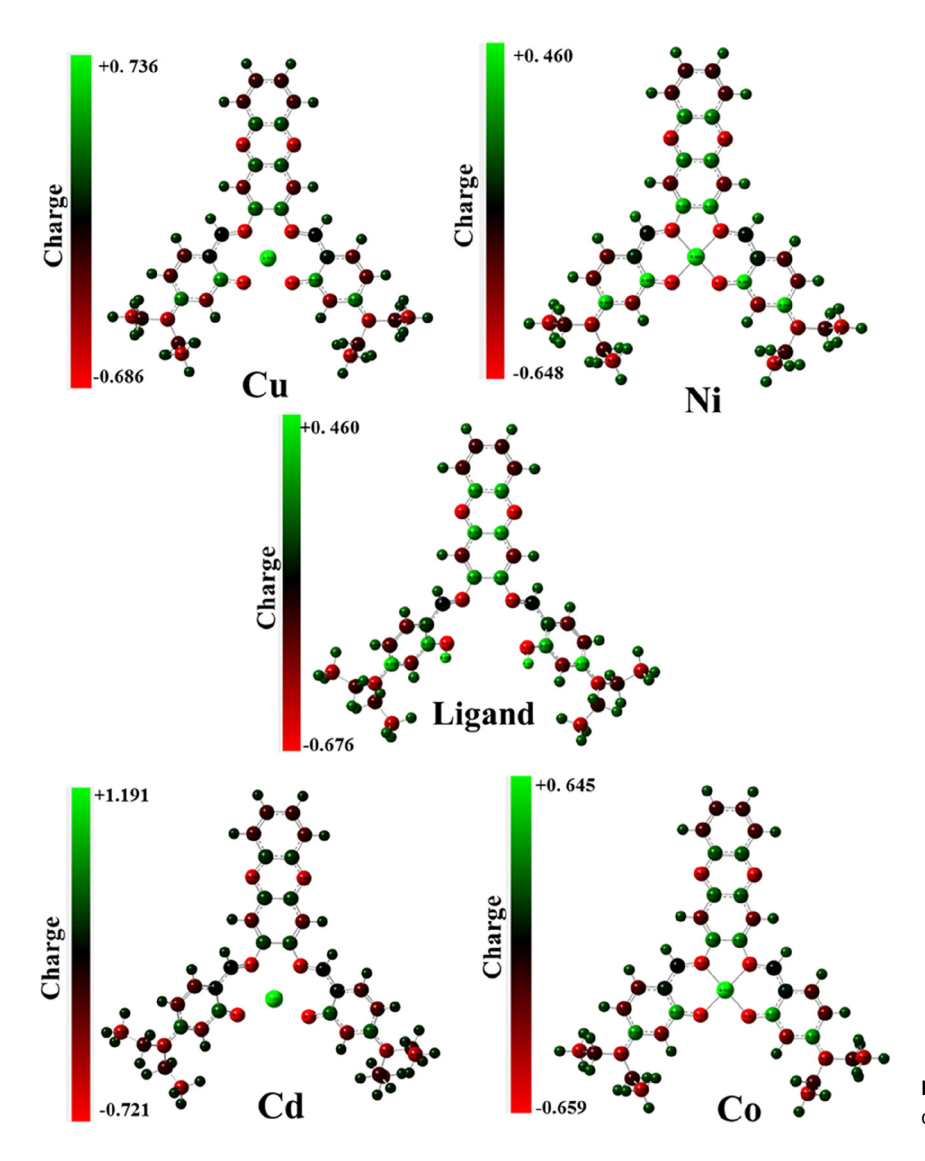


Figure 6: Molecular electrostatic potential map of compounds.

Table 10: Antimicrobial activity of the investigated complexes.

Compound	Antimicrobial activity (inhibition zone diameter in mm)								
	B. subtilis (+G)	S. aureus (+G)	E. coli (-G)	P. aeruginosa (–G)	A. flavus (fungus)	C. albicans (fungus)			
DMSO, control	NA	NA	NA	NA	_	_			
Ciprofloxacin	7	5	7	7	_	-			
Tetracycline	27	28	32	23	_	-			
Amphotericin B	_	_	_	_	21	20			
HL	25	30	18	14	7	5			
C1	36	33	24	22	5	5			
C2	28	30	24	26	8	8			
C3	28	32	25	24	14	14			
C4	38	37	28	16	7	27			

3.12.5 Anti-tritubercular activity

In vitro, the activity of the compounds and standard drug against *M. tuberculosis* was evaluated using the proportion

method, ²⁷ PZA was used as a positive control, and the results obtained were quite encouraging. The findings are listed in Table 13. Among the compounds examined, **C4** was found to be the most effective, followed by **C2**, which showed higher

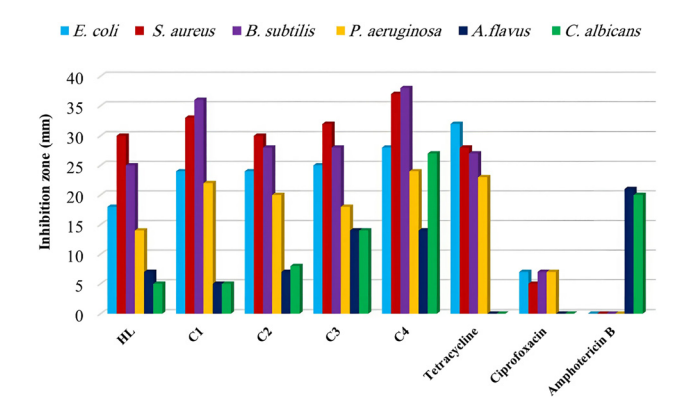


Figure 7: Antimicrobial activity of the compounds and standard drugs.

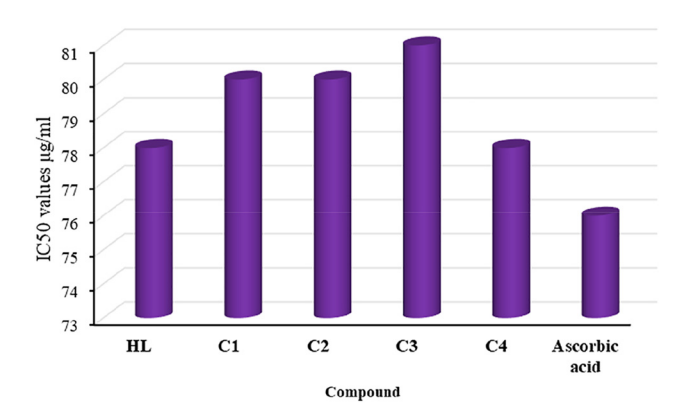


Figure 8: Antioxidant activity of compounds and standard (ascorbic acid).

Table 11: Cytotoxicity assay of ligand and their complexes.

Compound	LD ₅₀ (M mL ⁻¹)
HL	2.307×10^{-4}
C1	2.216×10^{-4}
C2	1.836×10^{-4}
C3	2.263×10^{-4}
C4	1.157×10^{-4}
Bleomycin	0.513×10^{-4}

Table 12: Anti-inflammatory activity of ligand and their complexes.

 23.86 ± 0.02

Diclofenac sodium

Symbol Inhibition % ± SD 25 50 100 200 15 H_2L 17.93 ± 0.02 20.68 ± 0.05 24.97 ± 0.08 29.03 ± 0.06 34.51 ± 0.05 C1 16.59 ± 0.04 20.84 ± 0.04 25.03 ± 0.02 29.77 ± 0.05 34.86 ± 0.02 C2 18.57 ± 0.08 21.07 ± 0.06 25.18 ± 0.10 30.26 ± 0.05 35.18 ± 0.02 C3 19.23 ± 0.06 21.84 ± 0.09 26.15 ± 0.10 31.16 ± 0.07 35.93 ± 0.02 C4 21.07 ± 0.06 23.54 ± 0.03 27.94 ± 0.08 34.75 ± 0.06 40.08 ± 0.09

 33.16 ± 0.08

 29.57 ± 0.05

activity compared to PZA against *M. tuberculosis* (Figure 10). The rest compounds showed activity similar to that of the standard drug against tuberculosis.

3.13 Molecular docking

A molecular docking study was carried out using AutodockVina to simulate docking with the target amino acids of the protein (PDB ID:1DQZ) and verify the binding properties of the compounds designed as tuberculosis drugs (Figure 11).³¹ Table 14 summarizes the binding affinity and type of binding between compounds with active sites in the amino acids of the protein. The major residues of the diethylamine site and the phenazine moiety's aromatic ring form hydrophobic interactions via Pi-alkyl bonding, for Instance, VAL-B163 and PRO-B237. Pi-anion binding was only observed in C2, which interacts electrostatically through the aromatic ring of the phenazine moiety with ASP-B234. Based on the binding affinity values of the compounds prepared, we found that the highest value was obtained for compound C4.

The **C4** exhibited a higher binding capacity with the protein of *M. tuberculosis* compared to other compounds, as shown by docking studies, which is consistent with the laboratory results.

3.14 ADMET analysis

Many compounds cannot be used as medicine due to various reasons such as insufficient absorption, distribution, high levels of toxicity, or excretion. These effects are collectively known as ADMET.³⁰ To determine whether an organic ligand and its synthesized metal complexes have a toxic effect after ingestion or have a good pharmacokinetic profile, they need to be tested thoroughly. To calculate ADMET parameters, the AdmetSAR web server was used. The server calculates pharmacokinetic, pharmacodynamic parameters and human intestinal absorption, etc.³¹ The organic Schiff

 38.75 ± 0.02

 41.63 ± 0.02

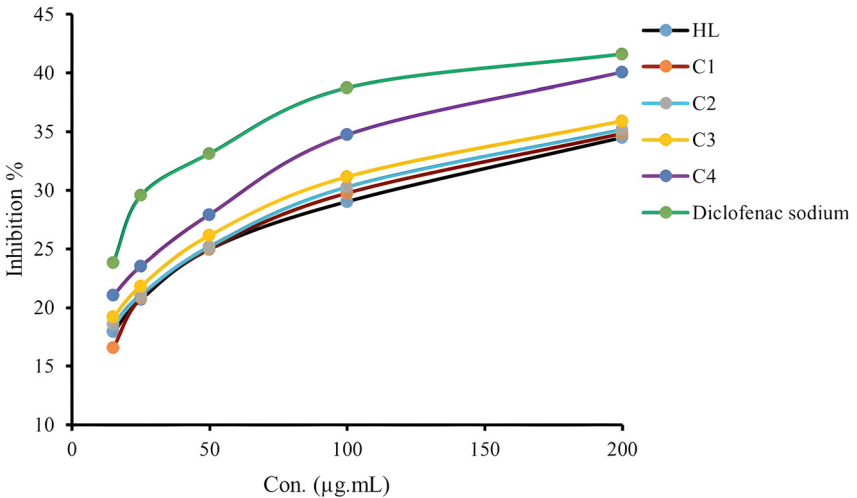


Figure 9: Anti-inflammatory activity of compounds and standard drug as % inhibition.

Table 13: Anti-tuberculosis activity data for compounds.

MIC (μg mL ⁻¹)
2.45 ± 0.018
3.16 ± 0.07
2.68 ± 0.10
2.74 ± 0.04
4.05 ± 0.05
3.2 ± 0.05

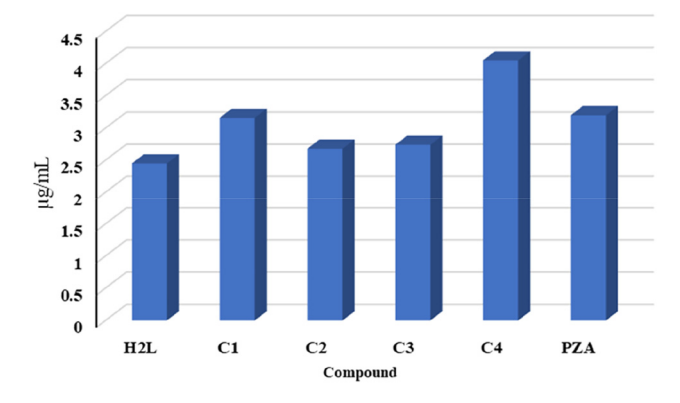


Figure 10: The antituberculosis activity of compounds and (PZA) standard drug.

ligand and its metal(II) complexes exhibit promising pharmacological properties for human intestinal absorption (Table 15). Negative values indicate a low *P*-glycoprotein inhibitor and CYP2D9, while the ligand and its metal complexes also show similar values for oral toxicity. Additionally, it is considered safer than some drugs that disrupt liver function as it exhibits negative results for hepatotoxicity. Although positive nephrotoxicity values are moderate but pose a still risk as a drug design.

4 Conclusions

In this current research, a new series of metal complexes was synthesized in the study using the Schiff base bond formed from 2,3-diaminophenazine and 4-diethylaminosalicyaldehyde. The organic ligand and its complexes with Co(II), Ni(II), Cu(II), and Cd(II) were then analyzed using various methods, including molar conductivity, melting point, elemental analysis, magnetic moment, ¹H and ¹³C NMR, FT-IR, UV-Vis, ESR, and mass spectra, to confirm their structural identification and other characterization details. These analyses confirmed the square planar geometry of the complexes, and thermal analysis data showed that the compounds are thermally stable up to 253 °C. Moreover, the therapeutic aspects of (H₂L, C1, C2, C3, and C4) were highlighted by careful screening and serial dilution for anti-tuberculosis activities, antimicrobial activity, antioxidant, inflammatory activity, and cytotoxicity, respectively, and reveal. The biological activity of the compound was enhanced by complexation and followed the activity order of C4 > C3 > C1 > C2. Antimicrobial activity highlights that C4 and C3 are the most active with values comparable to standard drugs. The comparison of antioxidant activity values revealed that C1 and C2 were more susceptible to oxidation defects, displaying similar values to ascorbic acid. In terms of anti-inflammatory activity, the ligand and C4 exhibited higher activity, with a value similar to that of the standard diclofenac sodium. Computational studies, including DFT, MESP, molecular docking, and ADMET analyses, supported the experimental results and indicated strong interaction potential and suitability as therapeutic agents. The Cd(II) complex (C4) demonstrated the highest biological response, highlighted by its binding capacity, electrophilicity, and dipole moment. MESP results

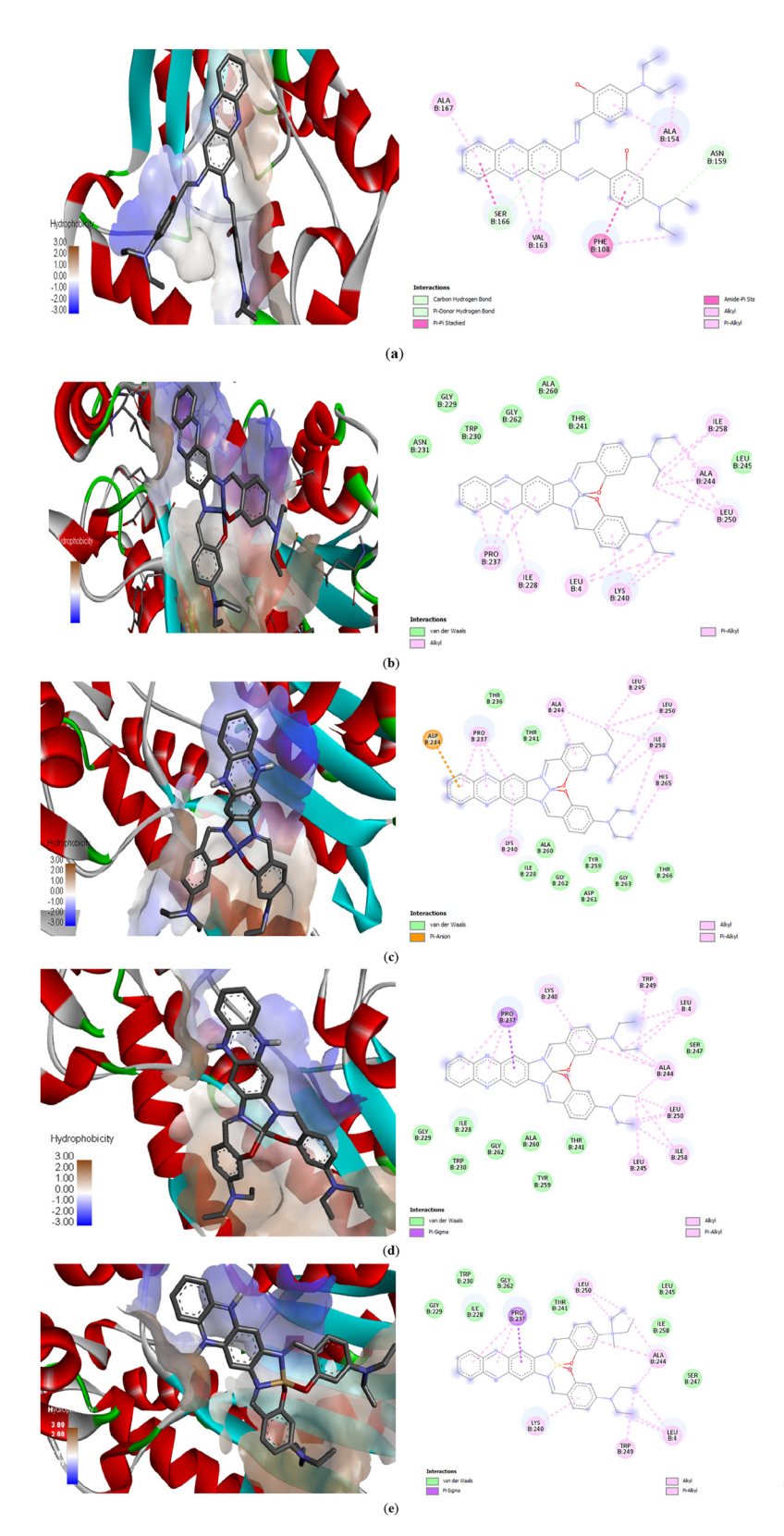


Figure 11: Predicted position of (a) H₂L; (b) C1; (c) C2; (d) C3; (e) C4 from docking analysis and binding interactions with amino acids.

corroborated the superior biological efficiency of the complexes compared to the ligand, and molecular docking studies confirmed that all synthesized compounds were more effective against tuberculosis than pyrazinamide, with the Cd(II) complex showing the highest docking affinity. ADMET analyses indicated that the compounds were free

Table 14: Physical features of ligand (HL) along with its complexes.

Compound Bonding affinity (kcal mol ⁻¹)		H₂L −6.9	C1 -7.8	C2	C3	C4 -8.4	
				-8.0	-8.0		
Hydrophobic	Pi-alkyl	ALA ^{B154} (4.89), VAL ^{B163} (5.04)	LYS ^{B240} (3.57), PRO ^{B237} (4.43), IEU ^{B258} (3.97)	LYS ^{B240} (5.39), PRO ^{B237} (00), ALA ^{B244} (3.82), LEU ^{B250} (3.98)	LYS ^{B240} (4.30)	LYS ^{B240} (4.59), ALA ^{B244} (4.15)	
	Pi- pi stacked	PHE ^{B108} (4.01)		()			
	Amide- pi stacked	PHE ^{B108} (4.60)					
	Alkyl	ALA ^{B154} (4.24)	ALA ^{B244} (4.09), LYS ^{B240} (3.60)	ALA ^{B244} (4.24), LEU ^{B245} (4.09), LEU ^{B250} (4.71), IEL ^{B258} (00)	LEU ^{B250} (4.65), LEU ^{B245} (4.32), ALA ^{B244} (3.48), LEU ^{B4} (4.70), TRP ^{B249} (4.98)	LEU ^{B250} (4.32), LEU ^{B4} (3.81), TRP ^{B249} (5.16)	
Van der waals			ASN ^{B231} (5.28), GLY ^{B229} (5.28), GLY ^{B262} (3.81), TRP ^{B230} (4.36), ALA ^{B260} (4.10, THR ^{B241} (3.59)			TRP ^{B230} (3.76), GLY ^{B229} (5.03), IEL ^{B228} (5.02), THR ^{B241} (4.59), SER ^{B247} (5.16)	
Pi-sigma				. == B234	PRO ^{B237} (3.76)	(51.6)	
Pi-anion Conventional hydrogen bond				ASP ^{B234} (4.43)		ASN ^{B159} (3.41), SER ^{B166} (4.22)	

Table 15: ADMET parameter of the ligand and its complexes.

Parameter	H ₂ L	C1	C2	С3	C4
ADMET CYP2D6	(-)	(-)	(-)	(-)	(-)
	0.7022	0.7705	0.7705	0.7694	0.7694
ADMET CYP2D9	(-)	(-)	(-)	(-)	(-)
	0.6265	0.5707	0.5707	0.5710	0.5710
ADMET hepatoxicity	(-)	(-)	(-)	(-)	(+)
	0.5697	0.5322	0.5197	0.5697	0.5428
ADMET	(+)	(+)	(+)	(+)	(+)
nephrotoxicity	0.6601	0.6933	0.6559	0.6053	0.8150
P-Glucoprotien	(+)	(+)	(+)	(+)	(+)
inhibitor	0.8539	0.8772	0.8770	0.8772	0.8772
Acute oral toxicity	(III)	(III)	(III)	(III)	(III)
	0.6300	0.5904	0.5903	0.5904	0.5904
Human intestinal	(+)	(+)	(+)	(+)	(+)
absorption	0.9475	0.9580	0.9579	0.9580	0.9580

from immunological, hepatic toxicity, and mutagenicity concerns, although there was a cautionary indication of potential nephrotoxicity. This research showcases a new direction in the use of Schiff base compounds containing 2,3-diaminophenazine moiety as a potential treatment for tuberculosis.

Acknowledgments: The authors express acknowledgement to Departments for providing research facilities.

Research ethics: Not applicable.

Author contributions: Conceptualization, S.B., M.E. and A.A; methodology, R.E., M.B., H.A and A.A. .; software, M.B. D.T and F.B.; validation, S.B., D.T. and L.M.; formal analysis, R.E., L.E., R.A., and M.B; investigation, S.B., R.K. and D.T; resources, R.E. and S.B; data curation, S.B.; writing—original draft preparation, S.B. and M.E and D.T; writing-review and editing, R. E., F.B; visualization, S.B., D.T, F.B; supervision, S.B., M.E and F.B; project administration, R.E, L.M and A.A.; funding acquisition, R.E. and M.B. All authors have read and agreed to the published version of the manuscript.

Competing interests: The authors states no conflict of interest.

Research funding: None declared.

Data availability: The raw data can be obtained on request from the corresponding author.

References

1. Gilham, E. L.; Pearce-Smith, N.; Carter, V.; Ashiru-Oredope, D. Assessment of Global Antimicrobial Resistance Campaigns Conducted to Improve Public Awareness and Antimicrobial Use Behaviours: a Rapid Systematic Review. BMC Publ. Health 2024, 24, 396.

- 2. Ahmed, S. K.; Hussein, S.; Qurbani, K.; Ibrahim, R. H.; Fareeg, A.; Mahmood, K. A.; Mohamed, M. G. Antimicrobial Resistance: Impacts, Challenges, and Future Prospects. J. Med. Surg Public Health 2024, 2, 100081.
- 3. Sharma, V.; Das, R.; Mehta, D. K.; Sharma, D.; Aman, S.; Khan, M. Quinolone Scaffolds as Potential Drug Candidates against Infectious Microbes: a Review. Mol. Divers. 2024, 1-27; https://doi.org/10.1007/ s11030-024-10862-4.
- 4. Yakobi, S. H.; Magibile, Y. B.; Pooe, O. J. A Systematic Review of Neisseria Gonorrhoeae Drug Resistance Development in South Africa. Braz. J. Microbiol. 2024, 1-11; https://doi.org/10.1007/s42770-024-01281-
- 5. Pardo, L.; Mota, M. I.; Parnizari, A.; Varela, A.; Algorta, G.; Varela, G. Detection of Vancomycin Resistance Among Methicillin-Resistant Staphylococcus aureus Strains Recovered from Children with Invasive Diseases in a Reference Pediatric Hospital. Antibiotics 2024, 13, 298.
- 6. Okaiyeto, S. A.; Sutar, P. P.; Chen, C.; Ni, J.-B.; Wang, J.; Mujumdar, A. S.; Zhang, J.-S.; Xu, M.-Q.; Fang, X.-M.; Zhang, C.; Zhang, J. S.; Xu, M. Q.; Fang, X. M.; Xiao, H. W. Antibiotic Resistant Bacteria in Food Systems: Current Status, Resistance Mechanisms, and Mitigation Strategies. Agri. Commun. 2024, 100027; https://doi.org/10.1016/j.agrcom.2024. 100027.
- 7. Dheda, K.; Mirzayev, F.; Cirillo, D. M.; Udwadia, Z.; Dooley, K. E.; Chang, K.-C.; Omar, S. V.; Reuter, A.; Perumal, T.; Horsburgh, C. R. Jr.; Murray, M.; Lange, C. Multidrug-resistant Tuberculosis. Nat. Rev. Dis. Prim. 2024, 10, 22.
- 8. Kumari, N.; Sharma, R.; Ali, J.; Chandra, G.; Singh, S.; Krishnan, M. Y. The Use of Mycobacterium tuberculosis H37Ra-Infected Immunocompetent Mice as an In Vivo Model of Persisters. Tuberculosis 2024, 145, 102479.
- 9. Hu, X.; Liu, J.; Shao, Y.; Li, G.; Song, H.; Liu, Q.; Chen, C.; Zhu, L. Smoking Exposure and the Risk of Latent Tuberculosis Infection: Results from NHANES 2011-2012. Toxics 2024, 12, 94.
- 10. Hussein, H. A.; Ahmed, J. M.; Musse, A. H.; Gizaw, Y. Prevalence and Risk Factors of Bovine Tuberculosis in Cattle in Selected Districts of Fafan Pastoral Settings, Eastern Ethiopia. Heliyon 2024, 10; https://doi.org/10. 1016/j.heliyon.2024.e24998.
- 11. Kouengoua, A. P. K.; Tsissa, Y. L.; Noudeke, N. D.; Chimi, R. N.; Njayou, A.; Youssao, A. K. I.; Dahouda, M.; Boko, C.; Dougnon, V.; Awah-Ndukum, J.; Souaibou, F. Prevalence and Zoonotic Risk Factors of Mycobacterium Bovis Tuberculosis in Cattle at the Cattle-Wildlife-Human Interface in South and East Cameroon. Vet. World 2024, 17, 8.
- 12. El-Sonbati, A.; Omar, N.; Abou-Dobara, M.; Diab, M.; El-Mogazy, M.; Morgan, S. M.; Hussien, M.; El-Ghettany, A. Structural, Molecular Docking Computational Studies and In-Vitro Evidence for Antibacterial Activity of Mixed Ligand Complexes. J. Mol. Struct. 2021, 1239, 130481.
- 13. Bufarwa, S.; El-Seifat, R.; Binhamad, H.; Hesien, R. Synthesis, Characterization, Thermal, Theoretical Studies, Antimicrobial, Antioxidant Activity, Superoxide Dismutase-like Activity and Catalase Mimetics of Metal (II) Complexes Derived from Sugar and Schiff Base. Rev. Inorg. Chem. 2024, 44, 1-13.
- 14. Binhamad, H. A.; El-seifat, R. M.; Hesien, R. A.; Bufarw, S. M. Synthesis, Characterization (I.R, Elemental Analysis, Molar Conductivity), and Antibacterial Investigation of Complex Produced by the Reaction between Co(II) Ion with Mixed Ligands of (Amoxicillin and Salen). Al-Mukhtar J. Basic Sci. 2023, 21; https://doi.org/10.54172/4kk1ad33.
- 15. Almáši, M.; Vilková, M.; Bednarčík, J. Synthesis, Characterization and Spectral Properties of Novel Azo-Azomethine-Tetracarboxylic Schiff Base Ligand and its Co(II), Ni(II), Cu(II) and Pd(II) Complexes. Inorg. Chim. Acta. 2021, 515, 120064.

- 16. Anacona, J.; Santaella, J.; Al-Shemary, R. K. R.; Amenta, J.; Otero, A.; Ramos, C.; Celis, F. Ceftriaxone-based Schiff Base Transition Metal(II) Complexes. Synthesis, Characterization, Bacterial Toxicity, and DFT Calculations. Enhanced Antibacterial Activity of a Novel Zn(II) Complex against S. aureus and E. coli. J. Inorg. Biochem. 2021, 223, 111519.
- 17. Majumdar, D.; Philip, J. E.; Gassoumi, B.; Ayachi, S.; Abdelaziz, B.; Tüzün, B.; Roy, S. Supramolecular Clumps of μ2-1, 3-acetate Bridges of Cd(II)-Salen Complex: Synthesis, Spectroscopic Characterization, Crystal Structure, DFT Quantization's, and Antifungal Photodynamic Therapy. Heliyon 2024, 10, 1-21.
- 18. Sandhu, Q.-U.-A.; Pervaiz, M.; Majid, A.; Younas, U.; Saeed, Z.; Ashraf, A.; Khan, R. R. M.; Ullah, S.; Ali, F.; Jelani, S. Schiff Base Metal Complexes as Anti-inflammatory Agents. J. Coord. Chem. 2023, 76, 1094-1118.
- 19. Mohapatra, D.; Patra, S. A.; Pattanayak, P. D.; Sahu, G.; Sasamori, T.; Dinda, R. Monomeric Copper(II) Complexes with Unsymmetrical Salen Environment: Synthesis, Characterization and Study of Biological Activities. J. Inorg. Biochem. 2024, 253, 112497.
- 20. Sanjurani, T.; Paul, S.; Barman, P. Indole-based NNN Donor Schiff Base Ligand and its Complexes: Sonication-Assisted Synthesis, Characterization, DNA Binding, Anti-cancer Evaluation and In-Vitro Biological Assay. Bioorg. Chem. 2024, 107281; https://doi.org/10.1016/j. bioorg.2024.107281.
- 21. Kobus, M.; Friedrich, T.; Zorn, E.; Burmeister, N.; Maison, W. Medicinal Chemistry of Drugs with N-Oxide Functionalities. J. Med. Chem. 2024, 67, 5168-5184.
- 22. Chaudhary, A.; Khurana, J. M. Synthetic Routes for Phenazines: an Overview. Res. Chem. Intermed. 2018, 44, 1045-1083.
- 23. Abdolmaleki, A.; Tavakol, H.; Molavian, M. R.; Firouz, K. Synthesis, FT-IR, NMR and DFT Analysis of a New Salophen Based on Diaminophenazine Moiety. J. Mol. Struct. 2014, 1062, 44-47.
- 24. Saravanan, P.; Dusthackeer, V. A.; Rajmani, R.; Mahizhaveni, B.; Nirmal, C. R.; Rajadas, S. E.; Bhardwaj, N.; Ponnuraja, C.; Bhaskar, A.; Hemanthkumar, A.; Ramachandran, G.; Tripathy, S. P. Discovery of a Highly Potent Novel Rifampicin Analog by Preparing a Hybrid of the Precursors of the Antibiotic Drugs Rifampicin and Clofazimine, Sci. Rep. **2021**, 11, 1029.
- 25. Soekamto, N. H.; Okino, T.; Rasyid, H.; Pudjiastuti, P.; Hadisaputri, Y. E.; Zainul, R. Chemotherapeutic Prospects of Organic Extracts of Bornetella Nitida from Selayar Island. Kuwait J. Sci. 2024, 51, 100223.
- 26. Nithyabalaji, R.; Ramya, R. M.; Kavitha, R.; Radhakrishnan, K.; Kumar, J. V.; Al-Asbahi, B. A.; Dhananjaya, M.; Joo, S. W. Molecular Structure, Characterization, In Vitro and In-Silico Studies of N, N-Dimethyl Aminophenyl Schiff's Base-Chalcone Hybrid. Chem. Phys. Impact 2024, 8, 100422.
- 27. Dueke-Eze, C. U.; Fasina, T. M.; Oluwalana, A. E.; Familoni, O. B.; Mphalele, J. M.; Onubuogu, C. Synthesis and Biological Evaluation of Copper and Cobalt Complexes of (5-Substituted-Salicylidene) Isonicotinichydrazide Derivatives as Antitubercular Agents. Sci. Afr. 2020, 9, e00522.
- 28. Morgan, S. M.; Diab, M.; El-Sonbati, A. Supramolecular Assembly of Hydrogen Bonding, ESR Studies and Theoretical Calculations of Cu(II) Complexes. Appl. Organomet. Chem. 2018, 32, e4504.
- 29. Abou-Dobara, M. I.; Omar, N. F.; Diab, M. A.; El-Sonbati, A. Z.; Morgan, S. M.; El-Mogazy, M. A. Allyl Rhodanine Azo Dye Derivatives: Potential Antimicrobials Target D-alanyl Carrier Protein Ligase and Nucleoside Diphosphate Kinase. J. Cell. Biochem. 2019, 120, 1667-1678.
- 30. Kumar, B.; Devi, J.; Dubey, A.; Tufail, A.; Sharma, S. Exploring the Antimalarial, Antioxidant, Anti-inflammatory Activities of Newly

- Synthesized Transition Metal(II) Complexes Bearing Thiosemicarbazone Ligands: Insights from Molecular Docking, DFT, MESP and ADMET Studies. Inorg. Chem. Commun. 2024, 159, 111674.
- 31. Junaid, M.; Alam, M. J.; Hossain, M. K.; Halim, M. A.; Ullah, M. O. Molecular Docking and Dynamics of Nickel-Schiff Base Complexes for Inhibiting β-lactamase of Mycobacterium tuberculosis. Silico Pharmacol. 2018, 6, 1-11.
- 32. Al-Shemary, R. K.; Mohapatra, R. K.; Kumar, M.; Sarangi, A. K.; Azam, M.; Tuli, H. S.; Ansari, A.; Mohapatra, P. K.; Dhama, K. Synthesis, Structural Investigations, XRD, DFT, Anticancer and Molecular Docking Study of a Series of Thiazole Based Schiff Base Metal Complexes. J. Mol. Struct. **2023**, *1275*, 134676.
- 33. Shebl, M.; Adly, O. M.; El-Shafiy, H. F.; Khalil, S. M.; Taha, A.; Mahdi, M. A. Structural Variety of Mono-And Binuclear Transition Metal Complexes of 3-[(2-Hydroxy-Benzylidene)-Hydrazono]-1-(2-Hydroxyphenyl)-Butan-1-One: Synthesis, Spectral, Thermal, Molecular Modeling, Antimicrobial and Antitumor Studies. J. Mol. Struct. 2017, 1134, 649-660.
- 34. Amer, S.; El-Wakiel, N.; El-Ghamry, H. Synthesis, Spectral, Antitumor and Antimicrobial Studies on Cu(II) Complexes of Purine and Triazole Schiff Base Derivatives. J. Mol. Struct. 2013, 1049, 326-335.
- 35. Gaber, M.; El-Ghamry, H. A.; Fathalla, S. K.; Mansour, M. A. Synthesis, Spectroscopic, Thermal and Molecular Modeling Studies of Zn²⁺, Cd²⁺ and UO₂²⁺ Complexes of Schiff Bases Containing Triazole Moiety. Antimicrobial, Anticancer, Antioxidant and DNA Binding Studies. Mater. Sci. Eng. C 2018, 83, 78-89.
- 36. Tian, W.; Zhong, W.; Yang, Z.; Chen, L.; Lin, S.; Li, Y.; Wang, Y.; Yang, P.; Long, X. Synthesis, Characterization and Discovery of Multiple Anticancer Mechanisms of Dibutyltin Complexes Based on Salen-like Ligands. J. Inorg. Biochem. 2024, 251, 112434.
- 37. Al-Resayes, S. I.; Laria, F. Y.; Miloud, M. M.; El-ajaily, M. M.; El-Barasi, N. M.; Sarangi, A. K.; Verma, S.; Azam, M.; Seidel, V.; Mohapatra, R. K. Synthesis, Characterization, Biological Applications, and Molecular Docking Studies of Amino-Phenol-Derived Mixed-Ligand Complexes with Fe(III), Cr(III), and La(III) Ions. I. Saudi Chem. Soc. 2023, 27, 101622.
- 38. Bufarwa, S.: Abdel-Latif, S. Spectroscopic, Thermal, and Conductometric Studies of Some (Arylazo) Quinolin-8-Ol and Their Complexes with the Divalent Ions of Mn, Ni, Cu, and Zn. Eur. Chem. Bull. **2023**, *12*, 187-197.
- 39. Adly, O. M.; Shebl, M.; Abdelrhman, E. M.; El-Shetary, B. Structural Variety of Cu(II), Ni(II), and Co(II) Complexes of a Hydrazone Based on 5-acetyl-4-hydroxy-2H-1, 3-thiazine-2, 6 (3H)-dione: Synthesis, Spectroscopic, Density Functional Theory, Antitumor, and Docking Studies. Appl. Organomet. Chem. 2023, 37, e7036.
- 40. Khalil, M. H.; Abdullah, F. O. Synthesis, Characterisation, and Anticancer and Antioxidant Activities of Novel Complexes of Palladium and an Organic Schiff-Base Ligand. Bull. Chem. Soc. Ethiop. 2024, 38, 605-613.
- 41. Turomsha, I. S.; Gvozdev, M. Y.; Osipovich, N. P.; Staravoitava, V. A.; Shiman, D. I.; Loginova, N. V. Copper(II) Complexes of Sterically Hindered Phenolic Schiff Bases: Synthesis, Characterization, Interaction with Biomolecules, and Antioxidant and Antimicrobial Activity. New J. Chem. 2024; https://doi.org/10.1039/d4nj00430b.
- 42. Sousa, J. M.; Braz, E. M.; Bezerra, R. D.; Morais, A. I.; Vieira, A. C.; Costa, M. P.; Rizzo, M. S.; Chaves, L. L.; Barreto, H. M.; Osajima, J. A.; Silva-Filho, E. C. Study of the Antibacterial and Cytotoxic Activity of Chitosan and its Derivatives Chemically Modified with Phthalic Anhydride and Ethylenediamine. Int. J. Biol. Macromol. 2024, 130292; https://doi.org/10.1016/j.ijbiomac.2024.130292.
- 43. Al-Noor, T. H.; Mohapatra, R. K.; Azam, M.; Karem, L. K. A.; Mohapatra, P. K.; Ibrahim, A. A.; Parhi, P. K.; Dash, G. C.; El-ajaily, M. M.; Al-Resayes,

- S. I.; Raval, M. K.; Pintilie, L. Mixed-ligand Complexes of Ampicillin Derived Schiff Base Ligand and Nicotinamide: Synthesis, Physico-Chemical Studies, DFT Calculation, Antibacterial Study and Molecular Docking Analysis. J. Mol. Struct. 2021, 1229, 129832.
- 44. P. G. Lacroix, S. Di Bella, I. Ledoux, Synthesis and second-order nonlinear optical properties of new copper(II), nickel(II), and zinc(II) Schiff-base complexes. Toward a role of inorganic chromophores for second harmonic generation, Chem. Mater. 1996, 8, 541-545.
- 45. El-Sonbati, A. Z.; Diab, M. A.; Eldesoky, A. M.; Morgan, S. M.; Salem, O. L. Polymer Complexes. LXXVI. Synthesis, Characterization, CT-DNA Binding, Molecular Docking and Thermal Studies of Sulfoxine Polymer Complexes. Appl. Organomet. Chem. 2019, 33, e4839.
- 46. El-Sonbati, A.; Diab, M.; Morgan, S. M.; Abou-Dobara, M.; El-Ghettany, A. Synthesis, Characterization, Theoretical and Molecular Docking Studies of Mixed-Ligand Complexes of Cu(II), Ni(II), Co(II), Mn(II), Cr(III), UO₂(II) and Cd(II). J. Mol. Struct. 2020, 1200, 127065.
- 47. Abdelrhman, E. M.; El-Shetary, B.; Shebl, M.; Adly, O. M. Coordinating Behavior of Hydrazone Ligand Bearing Chromone Moiety towards Cu(II) Ions: Synthesis, Spectral, Density Functional Theory (DFT) Calculations, Antitumor, and Docking Studies. Appl. Organomet. Chem. 2021, 35, e6183.
- 48. Adly, O. M.; El-Shafiy, H. F.; Shebl, M. Synthesis, Spectroscopic Studies, DFT Calculations, Antimicrobial and Antitumor Activity of Tridentate NNO Schiff Base Metal Complexes Based on 5-Acetyl-4-Hydroxy-2h-1, 3-thiazine-2, 6 (3H)-Dione. J. Mol. Struct. 2019, 1196, 805-818.
- 49. Abbass, L. M.; Sadeek, S. A.; Zordok, W. A.-a.; Aziz, M. A. E.-R.; El-Attar, M. S. Mixed Ligand 4-hydroxy Acetanilide-Febuxostat Complexes of Co (II),-Ni (II), Cu (II) and Zr (IV): Synthesis, Structural Characterization, DFT Calculations, Antibacterial, Antioxidant and Molecular Docking Studies. J. Mol. Struct. 2024, 1308, 138115.
- 50. Omara, W.; Abdel-Latif, S. A.; Azzazy, H. M.; Abdel-Kader, N. S. Exploring Polyaniline Nanofilaments for Enhanced Optical Recognition of Lead in Water: An Integrated Approach of Experimental and Theoretical Studies. Appl. Organomet. Chem. 2024, 38, e7439.
- 51. El-Sonbati, A.: Diab, M.: El-Bindary, A.: Morgan, S. M. Supramolecular Spectroscopic and Thermal Studies of Azodye Complexes. Spectrochim. Acta Mol. Biomol. Spectrosc. 2014, 127, 310-328.
- 52. Mahmoud, W. H.; Sayed, F. N.; Mohamed, G. G. Azo Dye with Nitrogen Donor Sets of Atoms and its Metal Complexes: Synthesis, Characterization, DFT, Biological, Anticancer and Molecular Docking Studies. Appl. Organomet. Chem. 2018, 32, e4347.
- 53. Taxak, B.; Devi, J.; Dubey, A.; Kumar, B.; Tufail, A.; Pachwania, S.; Boora, A. Investigation of Anti-inflammatory and Antimicrobial Activities of Hydrazone-based Diorganotin (IV) Complexes: Synthesis, Spectroscopic Characterization, and Computational Studies. Appl. Organomet. Chem. 2024, 38, e7323.
- 54. Keypour, H.; Zeynali, H.; Fatemikia, H.; Ranjbar, N.; Karamian, R.; Rezaei, M. T.; Gable, R. W. Anticancer, Antioxidant, and Antimicrobial Studies and Molecular Docking of a New Hexanuclear Zn(II) Complex, Together with its X-Ray Crystal Analysis. Dalton Trans. 2024, 53, 4512-4525
- 55. Mamta, P.; Chaudhary, A. Novel Zn(II) Heterobimetallic Complexes: Synthesis, Characterization, Density Functional Theory Calculations, In Vitro Antimicrobial, Anti-inflammatory and Anticancer Activities. Res. Chem. Intermed. 2024, 1-31.

Supplementary Material: This article contains supplementary material (https://doi.org/10.1515/revic-2024-0007).